NUMERICAL SIMULATION OF FLOW OVER TWO-DIMENSIONAL HILLS USING A SECOND-ORDER TURBULENCE CLOSURE MODEL

R. YING and V. M. CANUTO
NASA, Goddard Institute for Space Studies, New York, NY 10025, U.S.A.

(Received in final form 17 June, 1997)

Abstract. We study turbulent flow over two-dimensional hills. The Reynolds stresses are represented by a second-order closure model, where advection, diffusion, production and dissipation processes are all accounted for. We solve a full set of primitive non-hydrostatic dynamic equations for mean flow quantities using a finite-difference numerical method. The model predictions for the mean velocity and Reynolds stresses are compared with the measured data from a wind-tunnel experiment that simulates the atmospheric boundary layer. The agreement is good. The performance of the second-order closure model is also compared with that of lower level turbulence models, including the eddy-viscosity model and algebraic Reynolds stress models. It is concluded that the present closure is a considerable improvement over the other models in representing various physical effects in flow over hills. The feasibility of running a finite-difference numerical simulation incorporating a full second-order closure model on an IBM workstation is also demonstrated.

Key words: Numerical simulation, Turbulence closure model, Complex terrain

1. Introduction

In the past, we have carried out a systematic study of the atmospheric boundary-layer (ABL) flow over hills using a variety of turbulence closure models. Specifically, we applied two algebraic Reynolds stress models (ARSMs): one is in a simplified form (Rodi, 1984; Ying et al., 1994) and the other is in a more sophisticated form (Pope, 1975; Ying and Canuto, 1995). The former was shown to be inadequate mainly because it failed to predict the observed difference between the normal stresses even in the flat terrain. Although the latter can satisfactorily predict the normal stresses in both flat and hill cases, it still has the following flaws:

(a) The model cannot predict the shear stress properly in the flow over hill cases;

(b) The model only applies to two-dimensional turbulent flows and its extention to three-dimensions is very cumbersome. The model's extension to three dimensions is important because complex terrains existing in reality, such as hills, valleys and buildings, are always three-dimensional. In order to describe turbulent flows over realistic three-dimensional terrain, it is necessary to develop ultimately three-dimensional theoretical modelling and numerical simulation techniques.

(c) In spite of its compact analytic form, Pope's model turns out to be computationally much more expensive than turbulence models based on the eddy-viscosity assumption.

In order to overcome the deficiencies of the ARSMs, we need to resort to more advanced turbulence closure models. Among them, there is a three-dimensional

Boundary-Layer Meteorology **85:** 447–474, 1997.

extension of Pope's model (Gatski and Speziale, 1993). This three-dimensional model, however, contains exceedingly lengthy algebraic expressions to the point where it would be difficult to code it into a computer program, and the entailed computations would be very expensive. Besides, it would not improve the performance in predicting the shear stress in two-dimensional cases.

At present, the general opinion is that among the various available turbulence models, the second-order closure model, in which each Reynolds stress component is solved by a separate differential equation, is the most reliable. Specifically, the advantages of the second-order closure model are

(a) The eddy viscosity hypothesis is no longer used so that the stresses are not closely tied to the mean velocity gradient.

(b) Advection, diffusion, production and dissipation processes are all included in each of the stress equations.

(c) In contrast to the one- or two-equation models (Rodi, 1984), this model allows for different evolutions of the various turbulent stresses (representing various velocity scales in complex flows).

(d) The formulation for two-dimensional and three-dimensional cases is unified. Thus, the transition from two-dimensional to three-dimensional simulations is straightforward.

The major concern with using second-order turbulence closure models in numerical simulations has always been that they are computationally expensive. Fortunately, in recent years, the advent and wide adoption of high performance workstations greatly eased this concern. In fact, nowadays simulations incorporating second-order closure turbulence models in a finite-difference numerical scheme are no longer formidable. In our opinion, along with the continuous development of the modern computers, this type of simulation is bound to become commonplace.

Since, as shown in Ying and Canuto (1995), the simplest turbulence model that promises success in predicting any difference between the normal stresses is Pope's ARSM, it is also of interest to compare the second-order closure model with Pope's model. Our work has shown, somewhat surprisingly, that running a full second-order closure model needs only a slightly longer CPU time than Pope's model. This fact confirms the computational feasibility of incorporating a second-order closure model in a two-dimensional numerical simulation.

The main purpose of this paper is to examine the predictions of a second-order closure turbulence model against wind-tunnel experimental data that simulate the atmospheric boundary layer. The specific wind-tunnel experiment we choose is the EPA experiment RUSHIL, which provides complete mean and turbulent field data for a neutrally stratified flow over isolated, two-dimensional hills of variable shape.

In the last two decades, the study of flow over hills has received considerable attention because of its importance in pollutant dispersion predictions and wind energy applications. In a most influential theoretical study of turbulent flow over hills (Jackson and Hunt, 1975), the flow is divided into two layers, an inner layer where the stress perturbation can affect the mean flow and an outer layer where the

flow is essentially inviscid. This theory has formed the basis for a series of models developed later (Mason and Sykes, 1979; Britter et al., 1981; Walmsley et al., 1982, 1986; Taylor et al., 1983; Hunt et al., 1988). The key to this approach is a careful scale analysis of the magnitudes of the various terms in the turbulence equation. It is known that at the bottom of the inner layer, the turbulence is approximately in local equilibrium, where the advection and transport are small, and the production is balanced by dissipation. In the outer layer, because the mean strain rates change rapidly compared to the eddy turnover time, the advection of the turbulent energy from upstream becomes important and there is no balance between production and dissipation. In Jackson and Hunt's work, the equation of motion is linearized so that it can only apply to flow over low hills. The analyses in this work, however, have had a profound influence on how to view flow over hills of steepness greater than the linearized approach strictly accommodates.

On the other hand, the numerical simulation method can solve the non-linear equations of motion with the addition of different turbulence closure schemes, and is not restricted to flow over low hills. Among the many authors who have carried out numerical simulations of flow over complex terrain, Beljaars et al. (1987) and Zeman and Jensen (1987) compared their computational results using different turbulence closure models to the Askervein field experimental data (Taylor and Teunissen, 1985). They concluded that only sophisticated closure models, such as the $E - \epsilon - \tau$ or the second-order closure, can correctly predict the stress changes over a hill. Ayotte et al. (1994) and Xu et al. (1994) compared the results of a variety of turbulence closure schemes for flow over complex terrain. Their results were not directly compared with measured data.

Reviewing the literature, we found that in the past, little attention had been paid to the study of the behaviour of normal stresses for flow over complex terrain. Also, the many measured Reynolds stress data in wind-tunnel experiments were rarely compared with simulation results. Our study will concentrate on these two aspects.

In this paper, we solve a full set of primitive non-hydrostatic dynamic equations for the mean flow quantities using a finite-difference method. The numerical code RAMS (the Regional Atmospheric Modelling System of Colorado State University) will be employed to perform the numerical calculation. The original RAMS code will be supplemented by the second-order turbulence closure model. To account for complex terrain, we use the terrain-following coordinate system available in RAMS (Clark, 1977), in which an irregular lower boundary is transformed into a plane. We shall make a detailed comparison of the simulation results with the wind-tunnel data, and assess the second-order closure model. The results will also be compared with our previous simulation results by using different, less advanced turbulence models.

2. Theoretical Formulation

2.1. NON-HYDROSTATIC FLOW MODEL OVER COMPLEX TERRAIN

The mean flow velocity is governed by the following equation of motion

$$\frac{d\overline{U_i}}{dt} + c_p\Theta_0\frac{\partial\pi'}{\partial x_i} = \delta_{i3}g\left(\frac{\overline{\Theta}}{\Theta_0} - 1\right) - \frac{\partial}{\partial x_j}\overline{u_i u_j}. \tag{1}$$

The pressure π' is determined by a non-hydrostatic equation

$$\frac{\partial\pi'}{\partial t} + \frac{R\Pi_0}{c_v\rho_0\Theta_0}\frac{\partial}{\partial x_j}(\rho_0\Theta_0\overline{U_j}) = 0. \tag{2}$$

In these equations, $\overline{U_i}$ and $\overline{\Theta}$ are the ensemble averages of the ith velocity component and the potential temperature respectively; ρ_0, Θ_0 and Π_0 are the density, potential temperature and dimensionless pressure of the initial unperturbed state of the atmosphere which is taken to be isentropic and at rest; π' is the deviation of the pressure from Π_0; $\overline{u_i u_j}$ are the Reynolds stresses; R is the gas constant for dry air; c_p and c_v are the specific heats at constant pressure and volume respectively and g is the acceleration due to gravity. For a detailed derivation and numerical solution procedures of the above equations, the reader is referred to Ying et al. (1994).

In the presence of complex terrain with surface height $z_g(x, y)$ and boundary layer height s, all equations are transformed from Cartesian coordinates (x, y, z) to a terrain following coordinate system (x, y, η) where

$$\eta = s\left[\frac{z - z_g(x, y)}{s - z_g(x, y)}\right]. \tag{3}$$

2.2. SECOND-ORDER CLOSURE TURBULENCE MODEL

In the second-order closure turbulence model, each component of the Reynolds stress tensor is solved by a separate transport equation. The exact transport equation for the Reynolds stress $\overline{u_i u_j}$ under neutral stratification has the form

$$\frac{d\overline{u_i u_j}}{dt} = \underbrace{-\frac{\partial}{\partial x_k}(\overline{u_i u_j u_k} + \delta_{jk}\overline{u_i p} + \delta_{ik}\overline{u_j p})}_{D_f(\overline{u_i u_j})=diffusion} \underbrace{-\left(\overline{u_j u_k}\frac{\partial\overline{U_i}}{\partial x_k} + \overline{u_i u_k}\frac{\partial\overline{U_j}}{\partial x_k}\right)}_{P_{ij}=stress\ \ production}$$

$$\underbrace{+\overline{p\left(\frac{\partial u_i}{\partial x_j} + \frac{\partial u_j}{\partial x_i}\right)}}_{\Pi_{ij}=pressure\ \ correlation} \quad \underbrace{-2\nu\overline{\frac{\partial u_i}{\partial x_k}\frac{\partial u_j}{\partial x_k}}}_{\epsilon_{ij}=dissipation}. \tag{4}$$

This equation provides a starting point for the set of equations used to determine the Reynolds stresses in the numerical simulation. To convert Equation (4) into a closed set of equations for the Reynolds stresses, the diffusion, pressure-correlation and dissipation terms must be modelled (deriving equations for these quantities merely introduces further unknown quantities). In our study, the diffusion term $D_f(\overline{u_i u_j})$ is taken to be of the down-gradient type model proposed by Daly and Harlow (1970)

$$D_f(\overline{u_i u_j}) = C_s \frac{\partial}{\partial x_l}\left(\frac{E}{\epsilon}\overline{u_k u_l}\frac{\partial \overline{u_i u_j}}{\partial x_k}\right). \tag{5}$$

The pressure-correlation term Π_{ij} can conveniently be separated into two parts,

$$\Pi_{ij} = \Pi_{ij,1} + \Pi_{ij,2}. \tag{6}$$

The first part $\Pi_{ij,1}$ is due to the turbulence-turbulence interactions (fast component) and the second part $\Pi_{ij,2}$ is due to the mean field-turbulence interactions (slow component). $\Pi_{ij,1}$ is expressed by a return-to-isotropy model (Rotta, 1951)

$$\Pi_{ij,1} = -C_1 \frac{\epsilon}{E} b_{ij}, \tag{7}$$

where

$$b_{ij} \equiv \overline{u_i u_j} - \frac{2}{3}\delta_{ij}E, \tag{8}$$

and C_1 is a constant. $\Pi_{ij,2}$ is modelled according to Launder, Reece and Rodi (1975)

$$\Pi_{ij,2} = \frac{4}{5}ES_{ij} + \frac{9C_2+6}{11}\left(b_{ik}S_{kj} + b_{jk}S_{ki} - \frac{2}{3}\delta_{ij}b_{lk}S_{kl}\right)$$

$$+\frac{7C_2-10}{11}\left(b_{ik}R_{kj} + b_{jk}R_{ki}\right), \tag{9}$$

where

$$S_{ij} \equiv \frac{1}{2}\left(\frac{\partial \overline{U_i}}{\partial x_j} + \frac{\partial \overline{U_j}}{\partial x_i}\right), \qquad R_{ij} \equiv \frac{1}{2}\left(\frac{\partial \overline{U_i}}{\partial x_j} - \frac{\partial \overline{U_j}}{\partial x_i}\right), \tag{10}$$

and C_2 is a constant.

The dissipation term ϵ_{ij} is modelled as

$$\epsilon_{ij} = -\frac{2}{3}\epsilon\delta_{ij}, \tag{11}$$

where ϵ is the total rate of energy dissipation.

In practice, the normal stresses appearing in the equations of the mean velocity components are not in the form of $\overline{u_i u_j}$ but b_{ij}. In fact, in formulating the mean velocity equations, the term $\overline{u_i u_j}$ is divided into two parts: $(\overline{u_i u_j} - \frac{2}{3}E\delta_{ij})$ and $\frac{2}{3}E\delta_{ij}$. The second part is absorbed in the pressure gradient term so that, in effect, the unknown static pressure p is replaced by $(p + \frac{2}{3}E\delta_{ij})$. Because of this, it is more convenient to formulate the differential equations in terms of b_{ij} instead of $\overline{u_i u_j}$. By taking the trace of Equation (4), we obtain the transport equation for E

$$\frac{dE}{dt} = D_f(E) + P - \epsilon, \tag{12}$$

where P is the production of E

$$P = -b_{ij} S_{ij}. \tag{13}$$

Incorporating Equation (12), the final form of the modelled differential equation for b_{ij} is

$$\begin{aligned} \frac{db_{ij}}{dt} \;=\; & D_f(b_{ij}) - C_1 \frac{\epsilon}{E} b_{ij} - b_1 E S_{ij} + \frac{9C_2 - 5}{11} \\ & \times \left(b_{ik} S_{kj} + b_{jk} S_{ki} - \frac{2}{3}\delta_{ij} b_{lk} S_{kl} \right) \\ & + \frac{7C_2 + 1}{11} \left(b_{ik} R_{kj} + b_{jk} R_{ki} \right). \end{aligned} \tag{14}$$

In deriving Equation (14), the production term in Equation (4) is written as

$$\begin{aligned} P_{ij} \;=\; & -\frac{4}{3} E S_{ij} - \left(b_{ik} S_{kj} + b_{jk} S_{ki} - \frac{2}{3}\delta_{ij} b_{lk} S_{kl} \right) \\ & - \left(b_{ik} R_{kj} + b_{jk} R_{ki} \right). \end{aligned} \tag{15}$$

Note that we added one adjustable parameter b_1 to the formulation following the argument of Jones and Musonge (1988) to fit the EPA wind-tunnel experimental data.

In our two-dimensional numerical simulation, we solve five differential equations for the turbulent quantities: $(\overline{u^2} - \frac{2}{3}E)$, $(\overline{w^2} - \frac{2}{3}E)$, $\overline{uw}$, E and ϵ; $(\overline{v^2} - \frac{2}{3}E)$ will be given by $-\left[(\overline{u^2} - \frac{2}{3}E) + (\overline{w^2} - \frac{2}{3}E)\right]$. We choose E instead of $\overline{v^2}$ because E is an important quantity to analyze and the equation for E is substantially simpler than that for $\overline{v^2}$.

2.3. TRANSPORT EQUATION FOR ϵ

The dissipation rate ϵ is governed by the following transport equation

$$\frac{d\epsilon}{dt} = C_\epsilon \frac{\partial}{\partial x_l} \left(\frac{E}{\epsilon} \overline{u_k u_l} \frac{\partial \epsilon}{\partial x_k} \right) + \frac{\epsilon}{E} (c_{1\epsilon} P - c_{2\epsilon} \epsilon), \tag{16}$$

where C_ϵ, $c_{1\epsilon}$ and $c_{2\epsilon}$ are constants. Among these constants, $c_{2\epsilon} = 1.92$ is a widely accepted value evaluated from measurement of decaying turbulence behind a grid, and the determination of the values of C_ϵ and $c_{1\epsilon}$ will be given later.

2.4. BOUNDARY CONDITIONS

In the second-order closure model, boundary conditions must be imposed on all the turbulent quantities on all four sides of the domain (in a two-dimensional case).

The same top boundary conditions apply to all the Reynolds stresses and ϵ, which is that the second spatial derivative of the variable in the direction normal to the boundary is zero. The lateral boundary conditions are also identical for all the Reynolds stresses and ϵ. At the inflow boundaries, the variable is kept constant in time. At the outflow boundaries, the second spatial derivative of the variable in the direction normal to the boundary is zero. At the lower boundary, we assume a similarity law for a constant-stress surface layer. First, we obtain the friction velocity u_* from the logarithmic profile of the mean velocity in the surface layer

$$\overline{U}(z_p) = \frac{u_*}{\kappa} \ln\left(\frac{z_p}{z_0}\right), \tag{17}$$

where z_p is some height within the surface layer, z_0 is the roughness length and $\kappa = 0.4$ is the Von Karman constant. The lower boundary condition for $\overline{uw}$ is simply

$$\overline{uw} = -u_*^2, \tag{18}$$

and that for ϵ is

$$\epsilon(z_p) = \frac{u_*^3}{\kappa z_p}. \tag{19}$$

The lower boundary conditions for the other turbulent quantities are more involved. First, in an equilibrium surface layer, if we neglect the transport terms in Equation (14), it reduces to a set of algebraic formulae for the Reynolds stresses

$$\frac{\overline{u^2}}{E} - \frac{2}{3} = \frac{12C_2 + 8}{33C_1}, \tag{20}$$

$$\frac{\overline{w^2}}{E} - \frac{2}{3} = \frac{2 - 30C_2}{33C_1}, \tag{21}$$

$$\left(\frac{\overline{uw}}{E}\right)^2 = \left(\frac{2}{3} + \frac{2 - 30C_2}{33C_1}\right)\frac{3 - C_2}{11C_1} + \frac{b_1}{2} - \left(\frac{2}{3} + \frac{12C_2 + 8}{33C_1}\right)\frac{8C_2 - 2}{11C_1}. \tag{22}$$

So, the boundary conditions for $\overline{u^2}$, $\overline{w^2}$ and E are dependent on the values of the three constants C_1, C_2 and b_1 appearing in the pressure-correlation tensor Π_{ij}.

The standard values of these parameters used in most applications were based upon extensive examination of engineering flows (Launder and Spalding, 1974). When these models are applied to the atmospheric boundary layer, the values of these constants inevitably need to be readjusted. In this study, we will use values that are in accordance with the observed data in the EPA experiment RUSHIL, which measured the Reynolds stresses near the surface as

$$\frac{\overline{u^2}}{E} - \frac{2}{3} = 0.384, \tag{23}$$

$$\frac{\overline{w^2}}{E} - \frac{2}{3} = -0.309, \tag{24}$$

and

$$\left(\frac{\overline{uw}}{E}\right)^2 = 0.182. \tag{25}$$

If we choose $C_1 = 1$, $C_2 = 0.4$ and $b_1 = 0.286$, Equations (20)–(22) give

$$\frac{\overline{u^2}}{E} - \frac{2}{3} = 0.388, \tag{26}$$

$$\frac{\overline{w^2}}{E} - \frac{2}{3} = -0.303, \tag{27}$$

and

$$\left(\frac{\overline{uw}}{E}\right)^2 = 0.182. \tag{28}$$

which are in good agreement with the experimental data. As a result, we use the following boundary conditions for $(\overline{u^2} - \frac{2}{3}E)$, $(\overline{w^2} - \frac{2}{3}E)$ and E

$$\overline{u^2} - \frac{2}{3}E = 2.11u_*^2, \tag{29}$$

$$\overline{w^2} - \frac{2}{3}E = -1.69u_*^2, \tag{30}$$

and

$$E = 5.48u_*^2. \tag{31}$$

We are aware that although we elaborately adjusted the values of C_1, C_2 and b_1 to reproduce the measured data, the approach is not entirely consistent with

the existence of a wall-reflection effect. Here, a brief discussion on this topic is in order.

In both homogeneous free shear flow and near-wall regions, the advection and diffusion of Reynolds stress are small, and production and dissipation are in balance. In its current form, the second-order closure model predicts the same stress ratios for both cases, as shown in Equations (20)–(22), but the experimentally measured values of these ratios are different. The discrepancy arises because, in formulating Launder et al.'s expression for the pressure correlation, a surface integral term, which corresponds to the pressure reflection from the wall, was neglected. Although this term does not contribute in a free shear flow, it does have a significant effect in the near-wall region.

To take into account this wall-reflection effect, several people have proposed near-wall correction terms to be added to the pressure correlation in the presence of a wall. Historically, however, the wall-correction terms proposed by many authors (Shir, 1973; Irwin, 1974; Launder et al., 1975; Gibson and Launder, 1978), were not successful. For example, Prud'homme (1984) found that for confined recirculating flows the wall term proposed by Launder et al. 'led to instability during computation and sometimes produced unrealistic relaminarization of the flow'. Newley (1985) found that adding the wall term admits non-unique or unstable solutions to the stress equations and it should be discarded. Xu et al. (1994) stated that when the wall correction term was included, no convergent solution could be obtained. A literature review shows that in the past, researchers were forced to exclude the wall correction terms in the Reynolds stress equations (Newley, 1985; Zeman and Jensen, 1987; Ayotte et al., 1994; Xu et al., 1994).

A common feature of all these wall-correction terms is that they introduce a dependence on parameters such as distance from the wall or wall-normal vectors into the closure. In handling flow in complex geometries, these parameters bring serious interpretational anomalies as well as give physically untenable behaviour. In an effort to eliminate these parameters from the closure, Launder and Li (1994) proposed a new formulation for the pressure-correlation term that incorporates the wall effect without adding an explicit wall-correction term. They claim that their new cubic model for the pressure correlation can mimic broadly the correct behaviour of the Reynolds stresses in both near-wall and free flows. Nevertheless, their formulation needs more testing, and also since the formulation contains many non-linear terms and is rather lengthy, it would be difficult to incorporate it into a numerical simulation program.

In summary, no satisfactory way to treat the wall-reflection effect in a numerical simulation is yet available. Thus, we performed our simulation without adding a wall-correction term to the pressure-correlation.

3. EPA Wind-Tunnel Experiment RUSHIL

The EPA wind-tunnel experiment RUSHIL (Khurshudyan et al., 1981) simulates a neutral atmospheric boundary layer with isolated two-dimensional hills. The incoming flow (in the x direction) is characterized by a logarithmic velocity profile

$$\overline{U}(z) = \frac{u_*}{\kappa} \ln\left(\frac{z}{z_0}\right), \tag{32}$$

with $z_0 = 0.157 \times 10^{-3}$ m and $u_* = 0.178$ m s^{-1}. This velocity profile reaches the free-stream velocity $U_\infty = 3.9$ m s^{-1} at the height of 1 m. A two-dimensional model hill of analytical shape is placed across the incoming flow, spanning the width of the tunnel (in the y direction). The shape of the hill is given by the following parametric equations:

$$x = \frac{1}{2}\xi\left[1 + \frac{a^2}{\xi^2 + m^2(a^2 - \xi^2)}\right], \quad |x| \le a \tag{33}$$

$$z = \frac{1}{2}m\sqrt{a^2 - \xi^2}\left[1 - \frac{a^2}{\xi^2 + m^2(a^2 - \xi^2)}\right], \tag{34}$$

where

$$m = \frac{h}{a} + \sqrt{\left(\frac{h}{a}\right) + 1}, \tag{35}$$

h is the height of the hill, a is the half width of the hill and ξ is an arbitrary parameter. Three different model hills with $h = 0.117$ m and different slope angles were used. Their aspect ratio a/h had values 8, 5 and 3, corresponding to maximum slope angles of 10°, 16° and 26°, respectively. The aspect ratios will be used as the hill identifier: Hill 8, Hill 5 and Hill 3.

Measurements of mean and turbulent velocity fields were made upwind, over and downwind of each of the hills. Vertical profiles of the mean horizontal velocity $\overline{U}(z)$, the angle of mean velocity to the horizontal surface $\Phi(z)$, the longitudinal and vertical (in Cartesian coordinates) turbulent intensities $\sigma_u(z)$ and $\sigma_w(z)$, and the Reynolds shear stress $\overline{uw}(z)$ were measured at 16 longitudinal locations from $x/a = -2$ to $x/a \ge 5$, where $x = 0$ corresponds to the top of the hill. For reference purposes, all the measurements were also made over the flat wind-tunnel floor.

4. Numerical Method

The modelled transport equations for $\overline{u_i u_j}$ coupled with the equations for the mean flow quantities were solved using a finite difference numerical method. In a finite

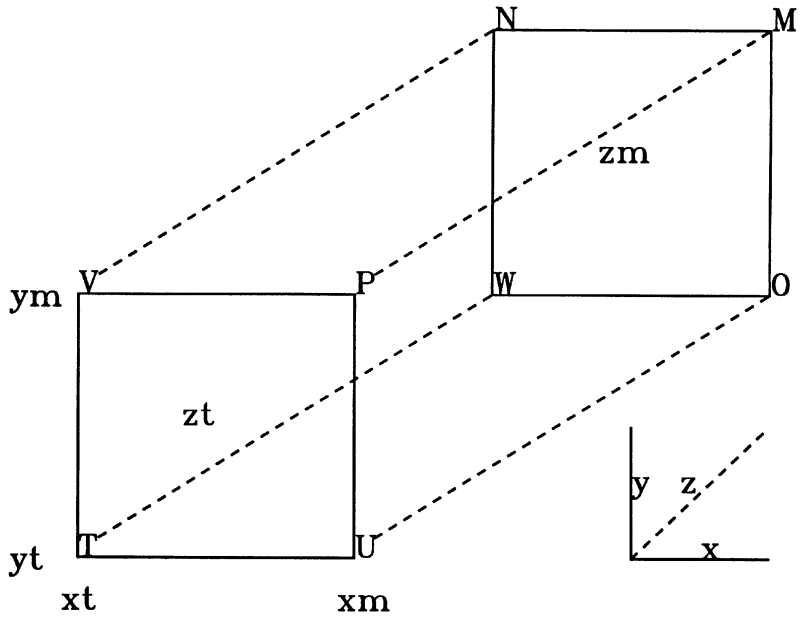

Figure 1. Schematic picture of the grid structure of the second-order closure model.

difference numerical scheme, all the equations must be discretized in both space and time. In the Arakawa C staggered grid system adopted by RAMS, we choose to hold the quantities $\overline{u^2}$, $\overline{w^2}$, $\overline{uw}$, $\overline{uv}$ and $\overline{vw}$ at the same grid locations as originally defined in RAMS when the eddy-viscosity formulae were used.

Since the grid system used in RAMS is rather complex, it is necessary to first clarify the grid system before discretizing the new equations for the Reynolds stresses. The grid points are staggered in all three coordinate directions. In the x-direction, the main grid points $xm(i)(i = 1, \cdots, N_1; N_1$ is the total grid points in the x-direction) span the whole computational domain, and the staggered grid point $xt(i)$ is defined at the middle point of $xm(i)$ and $xm(i-1)(i = 1, \cdots, N_1)$. Similarly, in the y-direction we have the main grid points $ym(i)$ and staggered grid points $yt(i)(i = 1, \cdots, N_2; N_2$ is the total grid points in the y-direction) and in the z-direction, $zm(i)$ and $zt(i)(i = 1, \cdots, N_3; N_3$ is the total grid points in the z-direction). Combination of these three staggered grid systems furnishes eight different sets of grid points at which a variable can be held. In the RAMS code, an upper letter is used to identify each of these eight sets of grid points. Figure 1 is a sketch of the grid structure and Table I indicates at which point a variable is being held.

Following standard practice, the value of a variable at a location where it is not stored is obtained by averaging adjacent values in the x-direction and/or y-direction and/or z-direction as appropriate. Averages are carried out before taking

Table I
Grid location of variables

Variable's name	Symbol	Grid Location
Mean velocity component in the x-direction	$\overline{U}$	U–point
Mean velocity component in the y-direction	$\overline{V}$	V–point
Mean velocity component in the z-direction	$\overline{W}$	W–point
Mean potential temperature	$\overline{\Theta}$	T–point
Turbulent kinetic energy	E	T–point
Energy dissipation rate	ϵ	T–point
Reynolds stress component	$\overline{u^2}$	T–point
Reynolds stress component	$\overline{w^2}$	T–point
Reynolds stress component	$\overline{uw}$	O–point
Reynolds stress component	$\overline{uv}$	P–point
Reynolds stress component	$\overline{vw}$	N–point
Air density	ρ	T–point
Dimensionless pressure	π	T–point

derivatives. In RAMS, all averages and derivatives are computed by calling the corresponding RAMS subroutines.

To obtain high vertical resolution near the ground and low resolution at higher levels, our model has the smallest grid increment near the ground, with the grid mesh expanding upward. In this vertically stretched grid, a constant expansion ratio is kept between the consecutive levels, which is equivalent to a logarithmic scaling commonly used in the ABL modeling. The expansion ratio, however, is set to a small value of 1.1 because large ratio would destroy the second-order accuracy of the vertical differencing in the model. In this way the vertical grid size is set to 0.005 m at the lowest level and stretched to 0.1 m at the level of 1m; above 1 m, the grid size remains constant at 0.1 m. We conducted sufficient sensitivity tests with different grid spacing and structure including the use of coarse, fine, uniformly spaced and stretched grids.

5. Simulations of the Mean and Turbulent Velocity Fields over Flat Terrain

There are a number of parameters in the second-order closure model, some of which we have already chosen using the boundary conditions for the Reynolds stresses by referring to the experimental data. In the process of determining the values of the remaining constants, we first introduce a relationship between constants $c_{1\epsilon}$, $c_{2\epsilon}$ and C_ϵ,

$$C_\epsilon = (c_{2\epsilon} - c_{1\epsilon}) \frac{u_*^6}{\kappa^2 E^2 \overline{w^2}}, \tag{36}$$

which is the limiting form of Equation (16) in the equilibrium surface layer. Equation (36) is derived from Equation (16) by (a) neglecting the advection of ϵ, (b) setting $P = \epsilon$, (c) substituting $\overline{uw} = -u_*^2$, and (d) using a logarithmic profile for $\overline{U}$ in the form of Equation (32).

Then, we test our simulation in the case of flat terrain. Comparing with the measured data in RUSHIL, constants $c_{1\epsilon}$ in the ϵ-equation and C_s in the diffusion term of the Reynolds stress equation are determined through computer optimization. Specifically, in the simulation of mean and turbulent flows over flat terrain, we have made many predictions of mean velocities and various turbulent quantities using a range of different values of $c_{1\epsilon}$ and C_s. With each given value of $c_{1\epsilon}$, the value of C_ϵ is given by Equation (36). We found that good agreement with the RUSHIL data can be achieved if we chose $c_{1\epsilon} = 0.94$, $C_\epsilon = 0.1$ and $C_s = 0.07$. These are our finally determined constant values.

In Figure 2, we give the predicted vertical profiles obtained from the simulations of the mean velocity $\overline{U}$, the shear stress $\overline{uw}$, and the turbulence intensities σ_u and σ_w over the flat floor using the constant values given above. In this paper, we present all the figures in a dimensionless form: the mean velocities $\overline{U}$ and $\overline{W}$ and the turbulent intensities σ_u and σ_w are normalized by the upstream friction velocity u_* given in Equation (32); the shear stress $\overline{uw}$ by u_*^2 and the height by the roughness length, z_0 also given in Equation (32). Figure 2 shows good agreement between the simulation results and measurements except some differences observed near the surface. Note that in Figures 2c and 2d, in order to show the remarkable improvement over the eddy viscosity assumption, we also plot the results given by the eddy viscosity assumption, i.e., $\sigma_u = \sigma_w = \sqrt{2E/3}$, with E given by the simulation results. It is clear that the second-order closure model can successfully predict the difference between the normal stresses, and is therefore in this respect superior to models based on the eddy-viscosity assumption.

6. Simulations of Turbulent Flow over Hills

The vertical profiles of the horizontal wind component $\overline{U}(z)$, the vertical wind component $\overline{W}(z)$, the turbulence intensities $\sigma_u(z)$ and $\sigma_w(z)$, and the Reynolds shear stress $\overline{uw}(z)$ computed for Hills 8, 5 and 3 using the second-order closure model, were compared with all available experimental profiles at 16 longitudinal locations.

As mentioned in the Introduction, the flow over hills can be divided into inner and outer layers. The justification of this division is the essentially different dynamical processes that dominate in each region. In brief, there are two fundamental time scales: the first one is the 'time of flight' T_a, which is the travel time for an eddy starting upstream to be advected along a streamline; the second is the turbulent time scale T_t, which is the time taken for an eddy to decay or turnover. The changes in the structure of turbulence over a hill depend on the relative magnitude of these

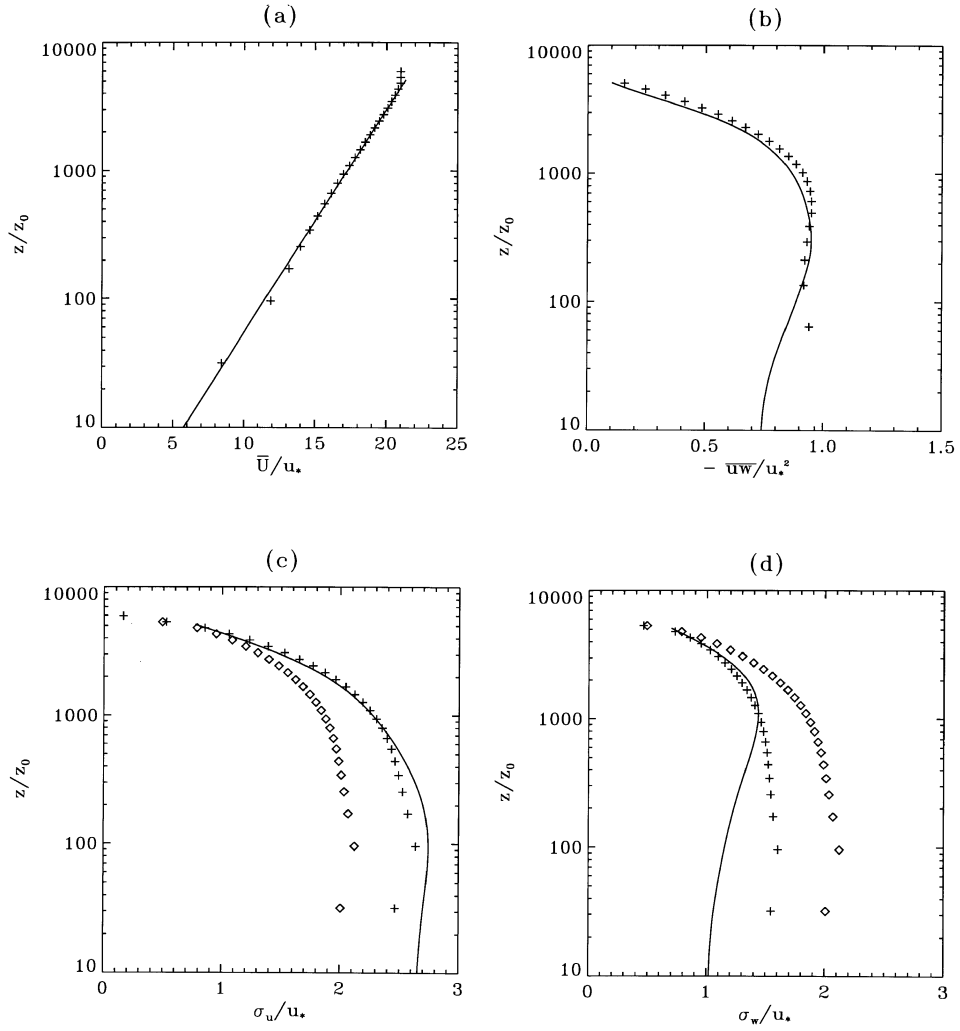

Figure 2. Vertical profiles of (a) the horizontal mean velocity $\overline{U}(z)$, (b) the Reynolds shear stress $\overline{uw}(z)$, (c) the longitudinal turbulence intensity $\sigma_u(z)$, and (d) the vertical turbulence intensity $\sigma_w(z)$ over flat terrain. The solid line is from the experimental data; the plus signs are the simulation results with the second-order closure model; the diamonds are the results from the eddy-viscosity approximation, where $\sigma_u(z) = \sigma_w(z) = 2E(z)/3$ with $E(z)$ given by simulations.

two scales. In the outer region, defined by $T_a < T_t$, the upstream boundary-layer turbulence is subject to rapid distortion. In the rapid distortion theory, it is assumed that in their life time the turbulence eddies have a chance to be rapidly distorted by the mean strain. In other words, the mean flow is changing too quickly for the turbulence to come into any kind of equilibrium with it. Consequently, in the outer region, the change in turbulence depend on the history of the mean flow and not on the local velocity gradient. In a thin inner layer adjacent to the surface, defined

by $T_a > T_t$, eddies encounter little change in the strain through their life time, so that the turbulence can reach an equilibrium with the perturbed mean flow. In this region, the turbulent production and dissipation dominate, and the condition for a local equilibrium is satisfied. In the intermediate region, where $T_a \sim T_t$, it is clear that the changes in the turbulence are diverse, i.e., the production, diffusion, advection, dissipation and the nonlinear process of pressure correlation are all of comparable importance. Therefore, the turbulence changes cannot be described by either rapid distortion or local equilibrium.

Based on this analysis, the height of the inner layer ℓ is defined as the height above the hill at which the turbulence time scale $T_t(\sim E/\epsilon)$ is roughly equal to the time of flight $T_a(\sim L/\overline{U})$, where L is the distance from the crest of the hill to the half-height position of the hill. Jackson and Hunt (1975) gave the following expression to determine ℓ

$$\frac{\ell}{L}\ln\left(\frac{\ell}{z_0}\right) = 2\kappa^2. \tag{37}$$

In presenting the results for flow over a hill, we labeled the inner layer height ℓ in all the graphs.

The simulation results for the mean velocity profiles $\overline{U}(z)$ and $\overline{W}(z)$ agree well with the wind-tunnel data and are insensitive to the particular closure scheme chosen. In Figures 3 and 4, we present the vertical profiles of $\overline{U}$ at three representative longitudinal locations (upstream, at hill top and downstream) obtained from the simulations with Hill 8 and Hill 5 using the second-order closure model. For comparison reason, the experimental data and the simulation results from Pope's model are also plotted. In addition, for reference purposes, the measured data in flat terrain are plotted in these and all the other vertical profile figures. The profiles drawn from flat terrain data serve as the reference upstream unperturbed profiles of the corresponding variables because in our simualation, we use the flat terrain data as the constant inflow boundary conditions for all the variables.

When presenting the simulation results for the Reynolds stresses, we need to point out that all the measurements over hills were made with hot-wire anemometers (HWA) (Khurshudyan et al., 1981). According to a report on another wind-tunnel experiment RUSVAL (Snyder et al., 1991), the HWA is a convenient instrument to use where the turbulence intensities are relatively low and the flow is not reversing. Since in the lee of Hill 3, the flows are highly turbulent and reversing, the measured data are likely to be erroneous. In this paper, to avoid the confusion caused by the doubtful measurements and concentrate on analyzing the model results of non-reversing flows, we present only the results of Reynolds stresses for Hill 8 and Hill 5.

In Figures 5 and 6, the vertical profiles of the longitudinal turbulence intensity σ_u at three representative longitudinal locations (upstream, at hill top and downstream) obtained from the simulations with Hill 8 and Hill 5 using the second-order closure model are compared with the corresponding measurements as well as the

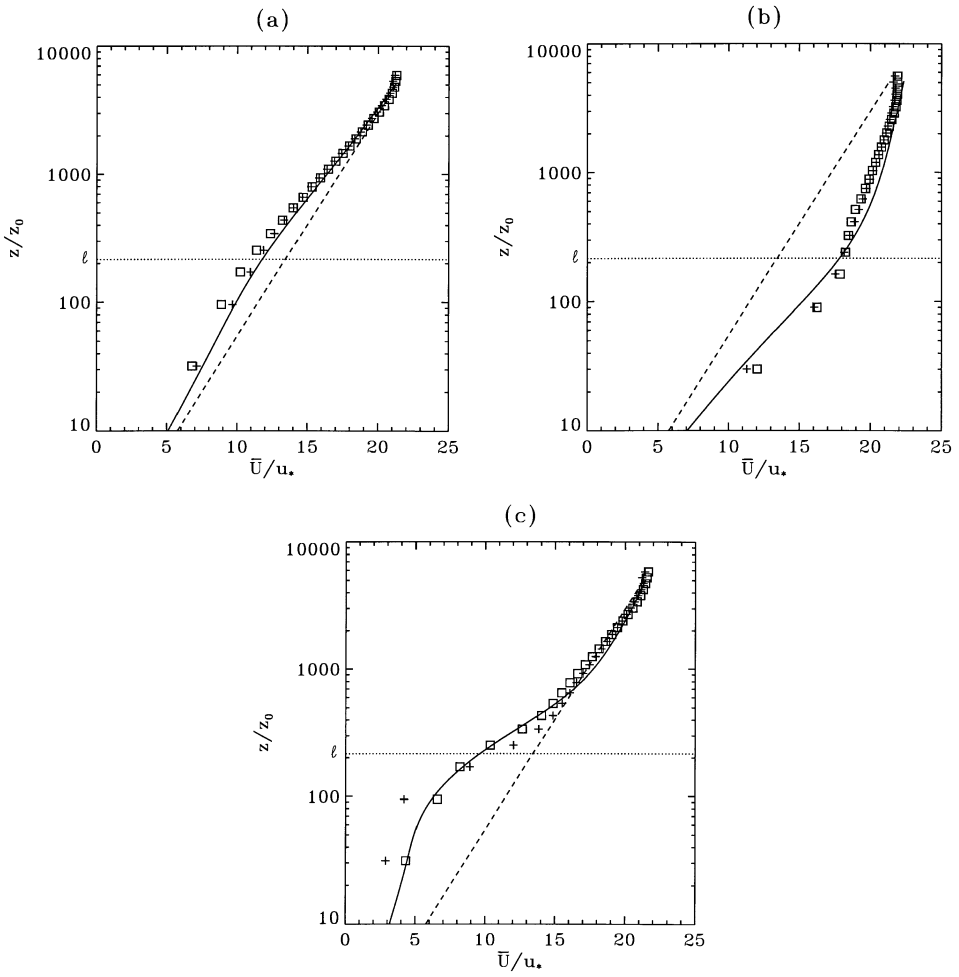

Figure 3. Vertical profiles of the horizontal mean velocity $\overline{U}(z)$ over Hill 8 at three longitudinal locations: (a) $x = -a$, (b)$x = 0$, (c) $x = 3a/4$. The solid line is from the experimental data for Hill 8; the dashed line is from the experimental data for flat terrain; the squares are the simulation results with Pope's model; the plus signs are the simulation results with the second-order closure model.

results from Pope's model. Overall, the model results are in very good agreement with the measurements. Moreover, the second-order closure model results show improvement over the Pope model.

In Figures 7 and 8, the modelled vertical profiles of the vertical turbulence intensity σ_w are compared with the corresponding measurements. The results from the second-order closure model for σ_w are slightly improved over those from Pope's model. Though both model results are acceptable, they don't quite follow the experimental trend of decreasing σ_w (as z decreases) in the inner layer. We have further studied this problem and noticed that this experimental trend appears consistently

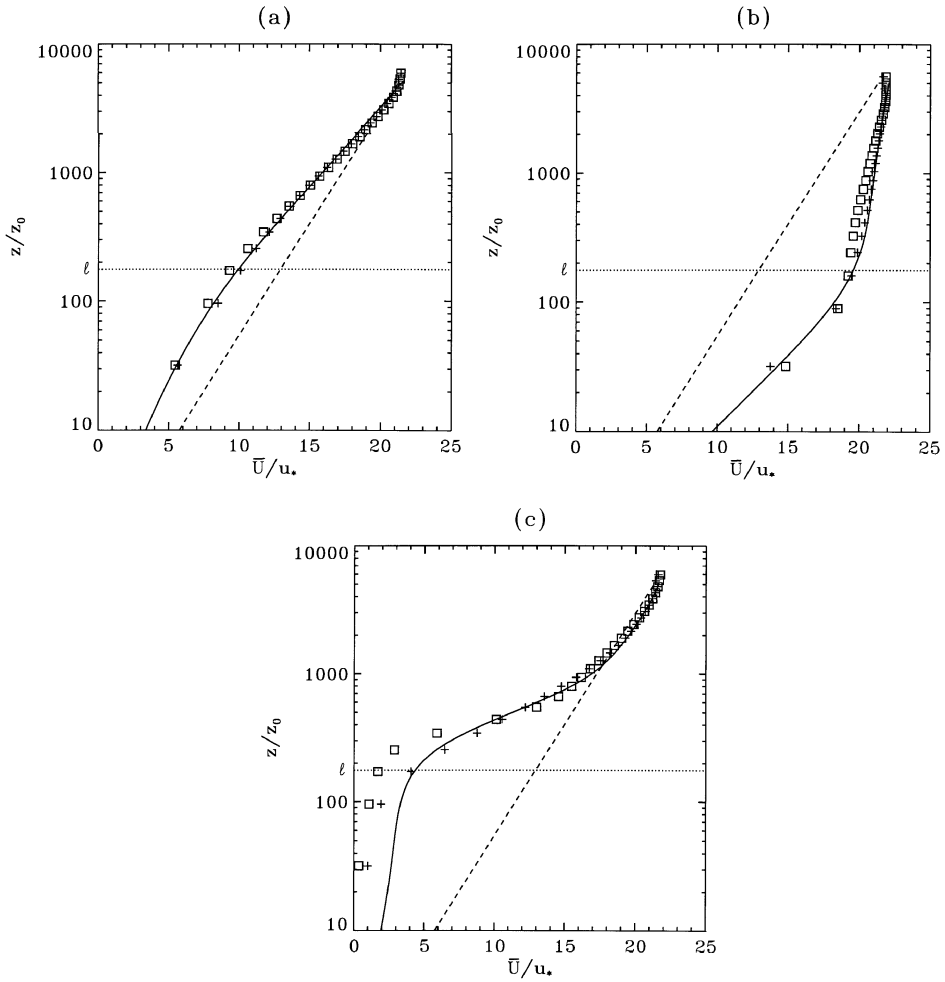

Figure 4. Vertical profiles of the horizontal mean velocity $\overline{U}(z)$ over Hill 5 at three longitudinal locations: (a) $x = -a$, (b)$x = 0$, (c) $x = a$. The solid line is from the experimental data for Hill 5; the dashed line is from the experimental data for flat terrain; the squares are the simulation results with Pope's model; the plus signs are the simulation results with the second-order closure model.

in the EPA and some other wind-tunnel experimental data (e.g., Finnigan et al., 1990). On the other hand, results from a series of different simulation studies (e.g., Newley, 1985; Zeman and Jensen, 1987) did not show such a feature. Since there is no evident physical mechanism that causes the vertical turbulent velocity to decrease sharply in the inner layer, we are inclined to attribute this discrepancy to experimental flaws rather than modelling problems.

Figures 9 and 10 show the model results of the vertical profiles of the shear stress $\overline{uw}(z)$ at three logitudinal locations of Hill 8 and Hill 5. Comparing with the RUSHIL experimental data, it is evident that at the hill top the values of $-\overline{uw}$

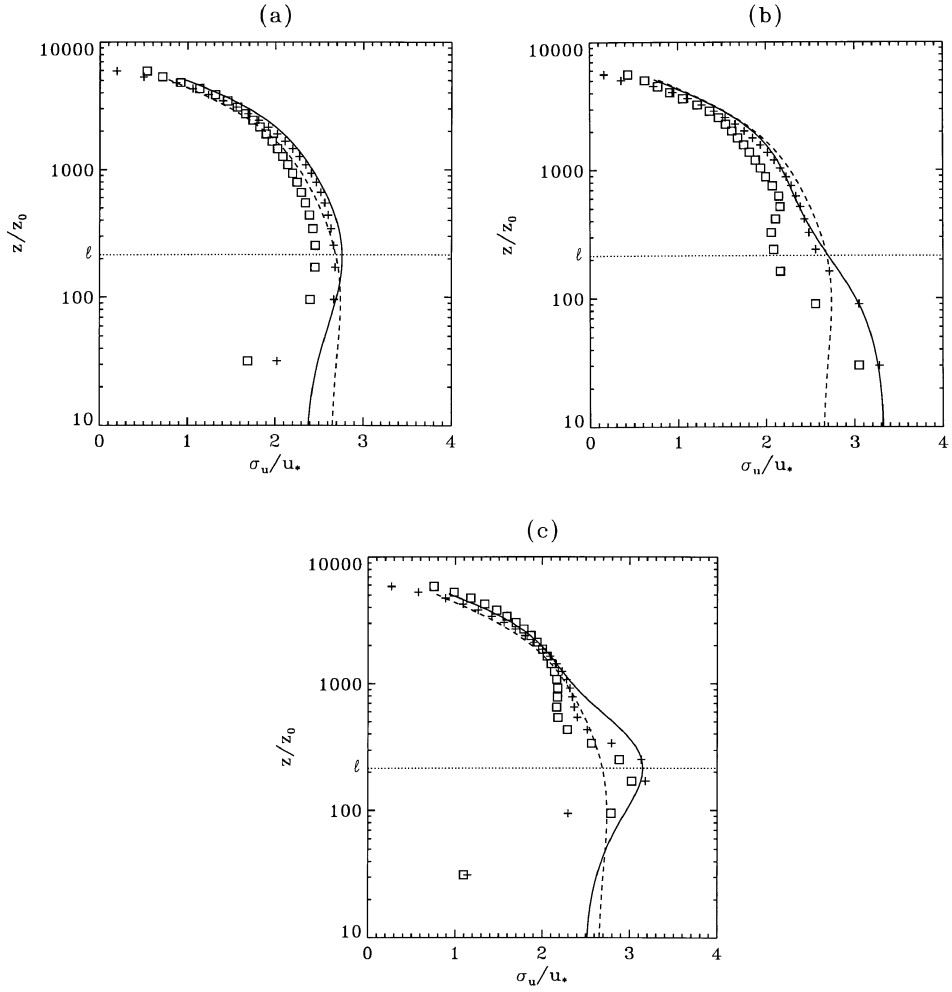

Figure 5. Same as Figure 3 but for the longitudinal turbulence intensity $\sigma_u(z)$.

predicted by Pope's model are too small. This disagreement should be attributed to an inadequate modelling of the turbulence transport terms in the $\overline{uw}$ equation, which involves the major approximation made in Pope's model. Since in the outer layer the advection of upstream turbulence has a dominant effect on the turbulence characteristics, an adequate modelling of the turbulence transport term is essential and more sophisticated models are needed to describe the behaviour of $\overline{uw}$. Figures 9 and 10 also show that the second-order closure model gives a dramatically improved performance over Pope's model, which indicates that its transport equation for $\overline{uw}$ can indeed adequately model the advection effect.

In the following, we will concentrate on the explanation of the model results in physical terms including the effects of local equilibrium, rapid distortion and

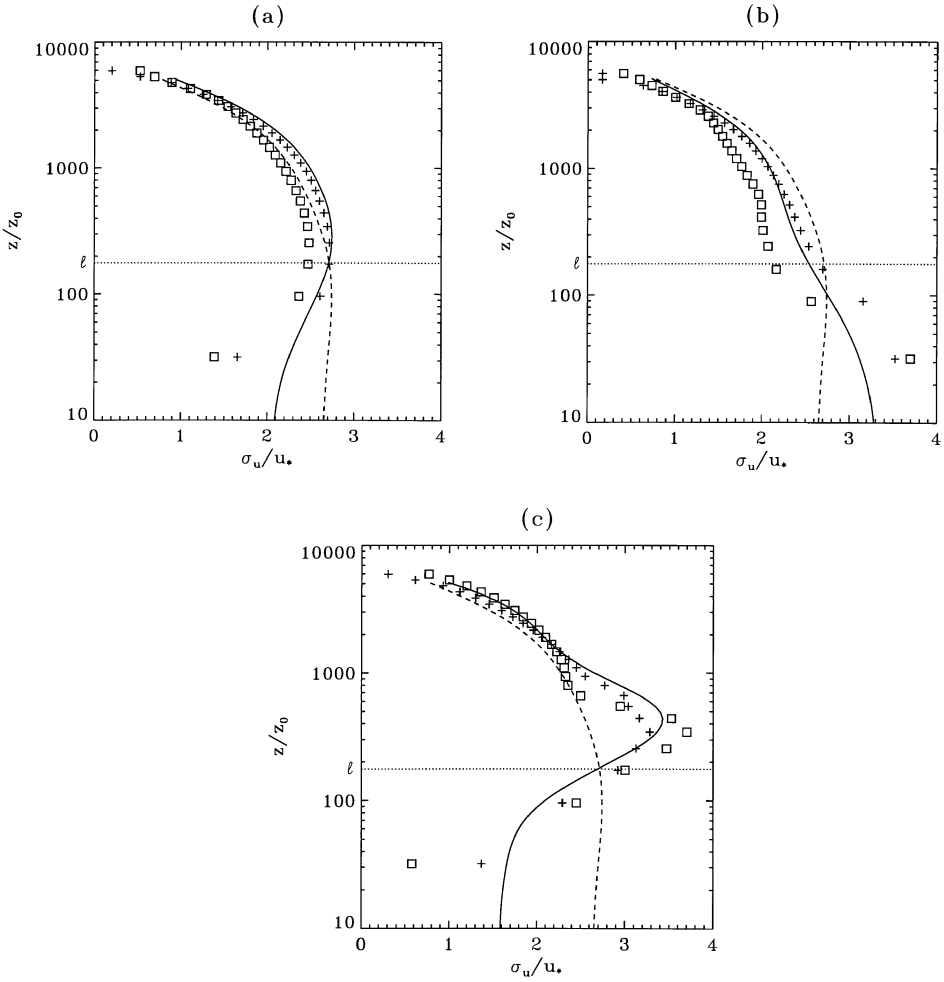

Figure 6. Same as Figure 4 but for the longitudinal turbulence intensity $\sigma_u(z)$.

streamline curvature. At the bottom of the inner layer, local equilibrium prevails. Local equilibrium, as mentioned before, is a state where production and dissipation are in balance, with advection and turbulent transport playing little part in the budget of the Reynolds stresses. Under these conditions, the eddy viscosity approximation would naturally apply. For example, in this region we should expect the shear stress $\overline{uw}$ to be proportional to the mean shear $\partial\overline{U}/\partial z$ and therefore closely related to the acceleration or deceleration of the mean flow.

In order to analyze the model results at the bottom of the inner layer, we resort to some streamwise profiles of Hill 8. Figures 11a and 11b show the profiles of σ_u and σ_w along a fixed $\eta = 0.005$ line of the terrain-following coordinate, which originates from the upstream height $z = 0.005$ m; and Figure 11c shows the profile

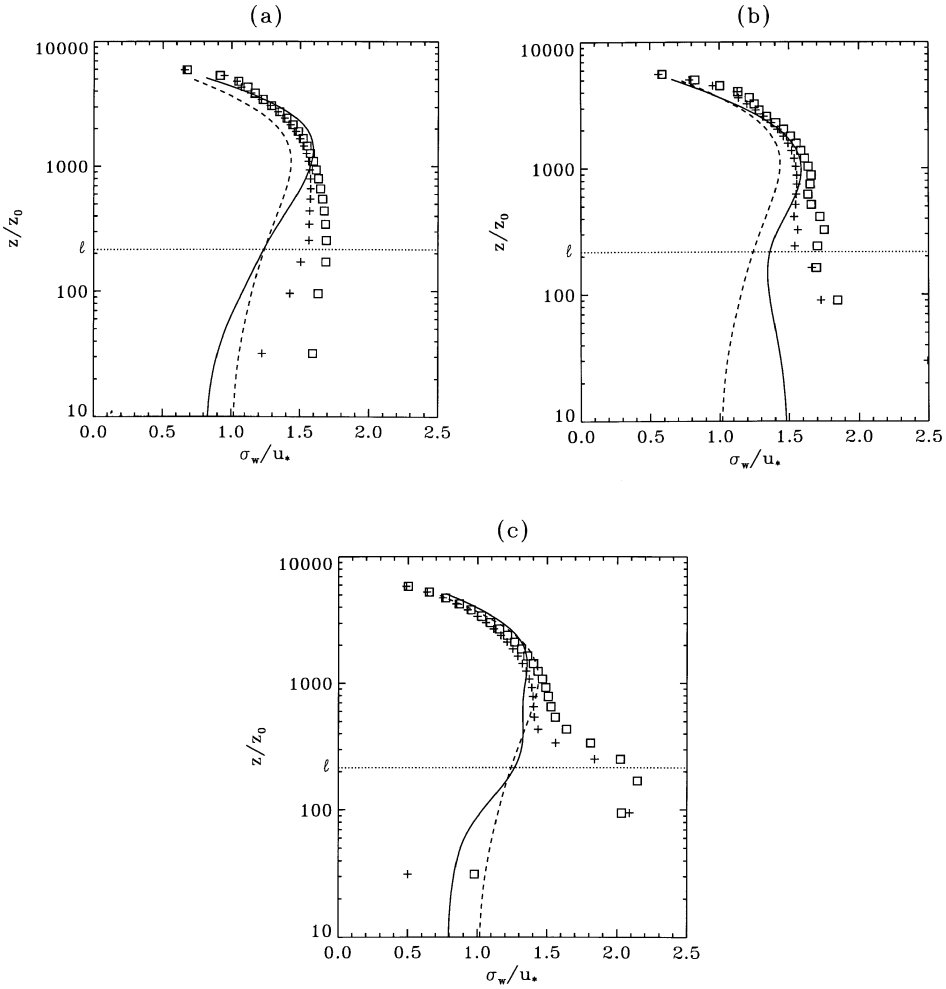

Figure 7. Same as Figure 3 but for the vertical turbulence intensity $\sigma_w(z)$.

of $\overline{uw}$ along the $\eta = 0$ line, which coincides with the surface. These profiles are all located at the bottom of the inner layer. Figure 3 shows the changes of the mean flow close to the surface, which can be summarized as the upstream deceleration, the speedup at the hill top and the deceleration in the lee. The model results clearly demonstrate that at the bottom of the inner layer, the changes of the Reynolds stresses over a hill reflect the changes of the mean shear near the surface. The upstream deceleration of the mean flow leads to a decrease of the Reynolds stresses; the speedup near the hill top leads to a big increase of the mean shear near the surface and a corresponding increase of the stresses, whereas the velocity reduction in the lee leads to a decrease of the stresses. In other words, these results are what we expect from the local equilibrium theory. When comparing the

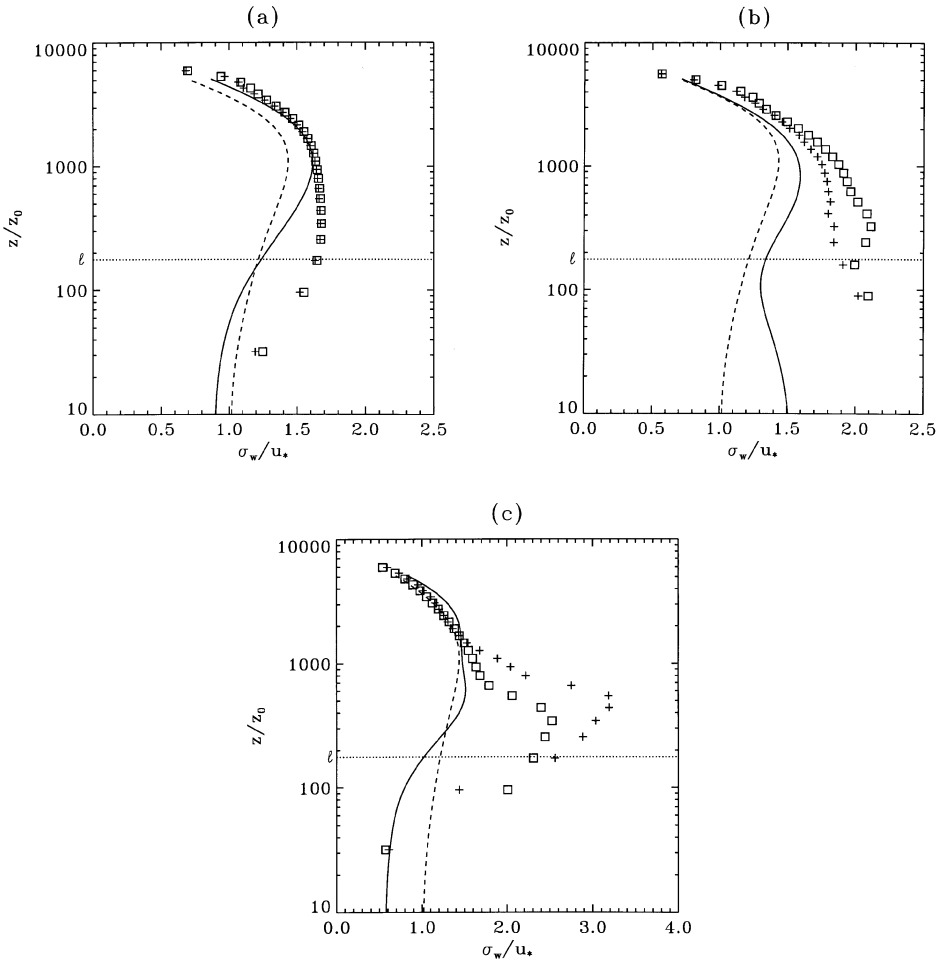

Figure 8. Same as Figure 4 but for the vertical turbulence intensity $\sigma_w(z)$.

model results with the wind-tunnel measurements, we find substantial differences between them. Moreover, the measured data do not reflect the changes in the flow speed well, especially in the case of σ_w and $\overline{uw}$. It is known that the roughness elements used in the RUSHIL experiment are river-washed gravels with diameters of about 0.01 m (Khurshudyan et al., 1982). Under this condition, measurements at a height of 0.005 m or less are almost impossible and the results are hardly reliable. In our opinion, for the most part one should probably disregard the experimental data in this case.

In the outer layer, the turbulence changes should be explained by the rapid distortion theory. Rapid distortion theory assumes that the distortion is sufficiently rapid so that an eddy has insufficient time to adjust to the local strain rate and to

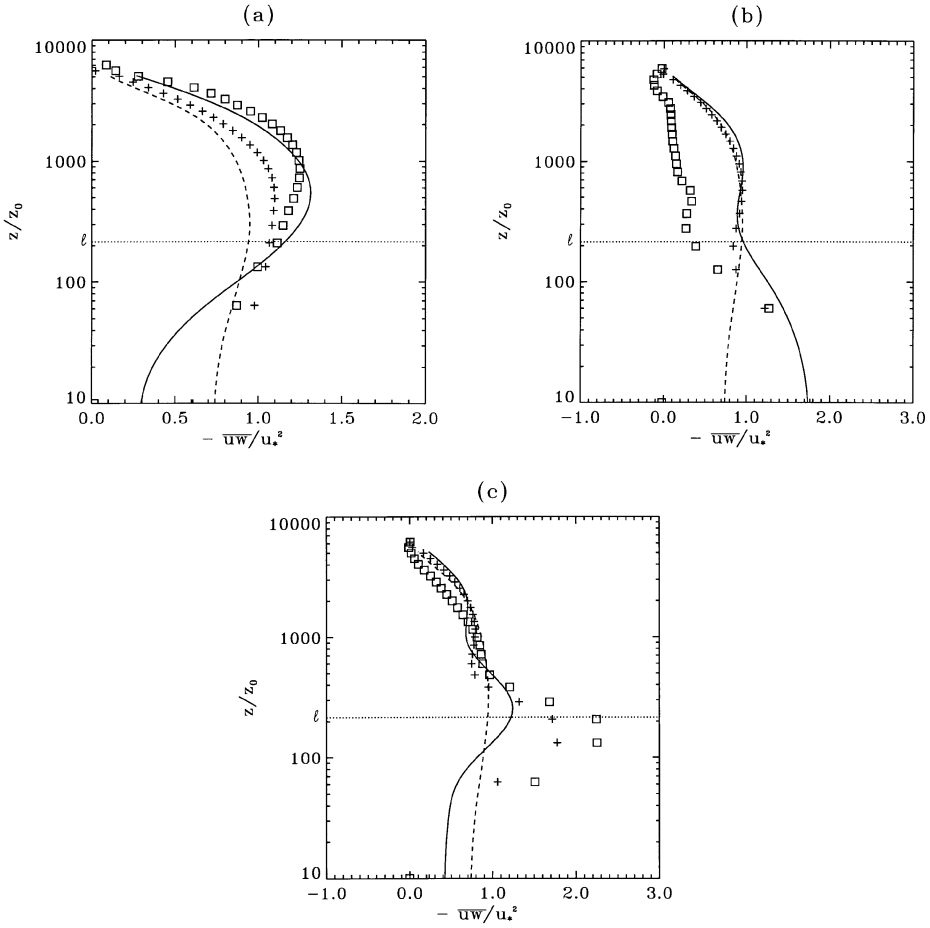

Figure 9. Same as Figure 3 but for the Reynolds stress $\overline{uw}(z)$.

interact with other eddies and the only effect on the turbulence from the distortion of the mean flow is to compress (or lengthen) and rotate individual vortex elements of the turbulence. For flow over a hill, Britter et al. (1981) gave a rapid distortion estimate of the changes in normal stresses for initially isotropic turbulence as

$$\frac{\overline{u^2} - \overline{u^2}_0}{\overline{u^2}_0} = -\frac{4}{5}\Delta S, \qquad \frac{\overline{w^2} - \overline{w^2}_0}{\overline{w^2}_0} = \frac{4}{5}\Delta S, \tag{38}$$

where the subscript 0 denotes the unperturbed upstream value of the quantity and ΔS is the fractional speedup given by

$$\Delta S = \frac{\overline{U} - \overline{U_0}}{\overline{U_0}}. \tag{39}$$

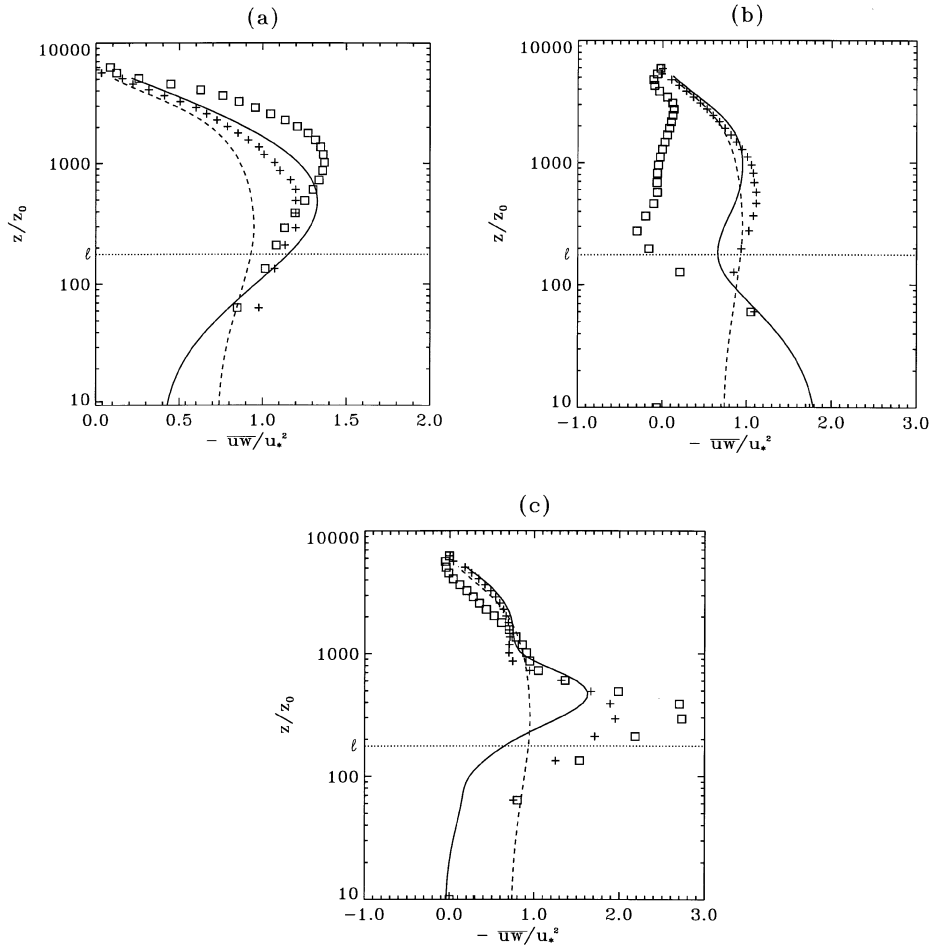

Figure 10. Same as Figure 4 but for the Reynolds stress $\overline{uw}(z)$.

It predicts a decrease in σ_u and an increase in σ_w at the hill top. Later, both Newley (1985) and Zeman and Jensen (1987) modified the above estimate for initially anisotropic turbulence. Newley derived the rapid distortion estimates for initially axisymmetric turbulence. His relationship for $\overline{u^2}$ is the same as Britter et al.'s and for $\overline{w^2}$ he gave

$$\frac{\overline{w^2} - \overline{w^2}_0}{\overline{w^2}_0} = \left(\frac{6}{5} - \frac{2}{5}A\right)\Delta S, \tag{40}$$

where $A = \overline{u^2}_0/\overline{w^2}_0$ is upstream anisotropy ratio.

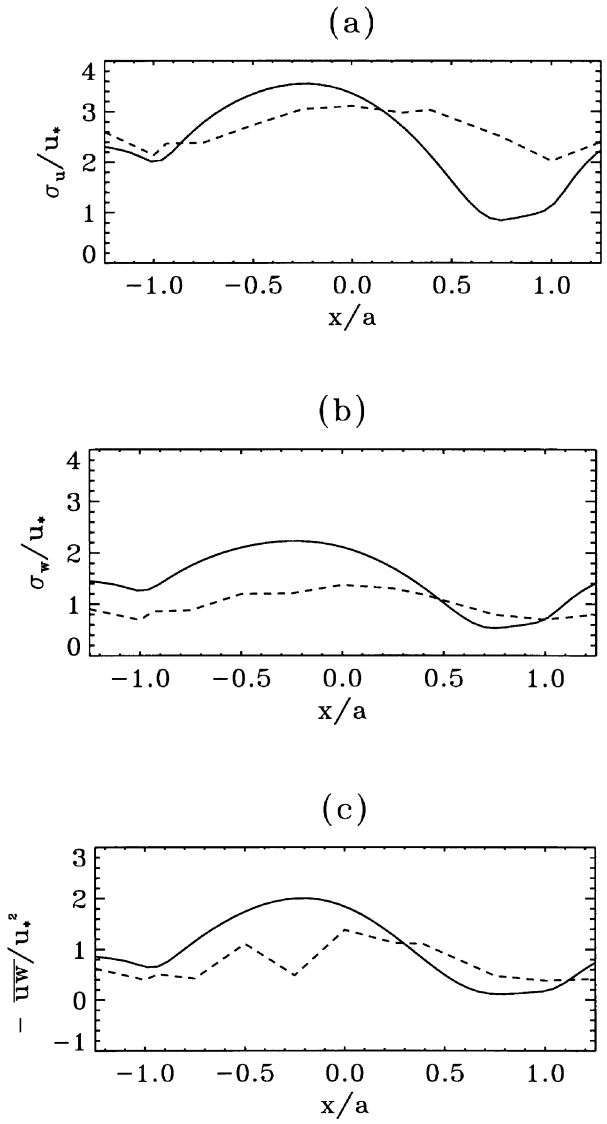

Figure 11. The streamwise profiles of the Reynolds stresses over Hill 8 along lines with constant η values: (a) for the longitudinal turbulence intensity $\sigma_u(x)$ with $\eta = 0.005$; (b) for the vertical turbulence intensity $\sigma_w(x)$ with $\eta = 0.005$; (c) for the Reynolds shear stress $\overline{uw}(x)$ with $\eta = 0$. The solid line is the simulation results with the second-order closure model; the dashed line is from the experimental data.

Incorporating their pressure correlation term, Zeman and Jensen derived the rapid distortion results for anisotropic upstream turbulence. Their result for $\overline{w^2}$ is the same as Newley's and for $\overline{u^2}$ they gave

$$\frac{\overline{u^2} - \overline{u^2}_0}{\overline{u^2}_0} = -\left(\frac{6}{5} - \frac{2}{5A}\right)\Delta S. \tag{41}$$

In summary, both results for initially anisotropic turbulence predict a decrease in σ_u for any value of A and an increase in σ_w for $A < 3$ at the hill top. The EPA wind-tunnel experimental data give $A < 2$, therefore we should expect a decreased σ_u and an increased σ_w at the hill top. Figures 5b, 6b, 7b and 8b show that both measured data and model results agree qualitatively with this estimate.

In order to show the curvature effects, in Figure 12, we present the streamwise profile of $\overline{uw}$ for Hill 8 along a fixed $\eta = 0.033$ line, which originates from the upstream height $z = 0.033$ m and is located near the inner-layer height ($\ell = 0.034$ m). There are two reasons why we choose this particular profile. The first reason can be seen from the transport equations for the Reynolds stresses written in a streamline coordinate system. Let x' and z' be the coordinates parallel and perpendicular to the flow direction respectively, $\overline{U'}$ be the mean velocity, $\overline{u'^2}$ and $\overline{w'^2}$ be the normal stresses in the x' and z' directions respectively, and $-\overline{u'w'}$ be the shear stress. According to Kaimal and Finnigan (1994), these equations are

$$\overline{U'}\frac{\partial \overline{u'^2}}{\partial x'} = -2\overline{u'^2}\frac{\partial \overline{U'}}{\partial x'} - 2\overline{u'w'}\frac{\partial \overline{U'}}{\partial z'} + 2\overline{u'w'}\left(\frac{\overline{U'}}{R}\right) + (\text{other terms}), \tag{42}$$

$$\overline{U'}\frac{\partial \overline{w'^2}}{\partial x'} = -4\overline{u'w'}\left(\frac{\overline{U'}}{R}\right) + 2\overline{w'^2}\frac{\partial \overline{U'}}{\partial x'} + (\text{other terms}), \tag{43}$$

$$\overline{U'}\frac{\partial \overline{u'w'}}{\partial x'} = -2\overline{u'^2}\left(\frac{\overline{U'}}{R}\right) + \overline{w'^2}\left(\frac{\overline{U'}}{R}\right) - \overline{w'^2}\frac{\partial \overline{U'}}{\partial z'} + (\text{other terms}), \tag{44}$$

where R is the radius of the streamline curvature, and (other terms) includes the diffusion, pressure-correlation and dissipation terms. It is evident that the advantage of writing the Reynolds stress equations in streamline coordinates is that the turbulence production is decoupled into individual terms, each of which can be identified with a certain physical effect, such as the streamwise flow acceleration $(\partial\overline{U'}/\partial x')$, the shear $(\partial\overline{U'}/\partial z')$ and the streamline curvature $(1/R)$. These equations show that only $\overline{u'w'}$ is dominated by the curvature effect (Kaimal and Finnigan, 1994), therefore we choose to present the profile of $\overline{uw}$ (which should have similar behaviour as $\overline{u'w'}$) in the Hill 8 case.

The second reason for presenting this profile is concerned with the height. As shown by Zeman and Jensen (1987), near the inner-outer layer interface (at $z = \ell$) the Reynolds stresses are most significantly affected by the streamline curvature, particularly near the hill top where the curvature dampens turbulence. This is because at higher levels the effect diminishes as the streamline curvature vanishes and at lower levels the mean shear becomes important.

In Figure 12, the model results of $-\overline{uw}$ show an increase at the upstream side of the hill, where the streamline curvature is concave, then a decrease over the hill top, where the curvature is convex, and finally an increase again in the lee, where the streamline curvature is again concave. Considering that in Equation (44) R is

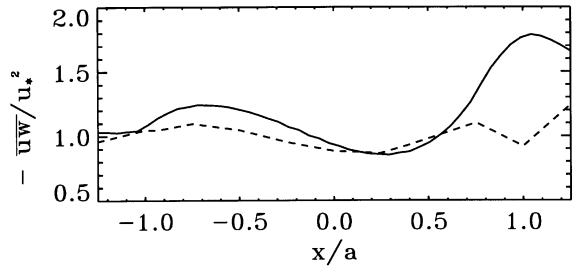

Figure 12. Same as Figure 11 for the Reynolds shear stress $\overline{uw}(x)$ with $\eta = 0.033$.

positive for a concave surface and negative for a convex surface, we conclude that the model results respond to the changes of curvature as the equation indicates. It is interesting to note that Busch et al. (1987) reached the same conclusion about the influence of curvature on the turbulence in hill flows using a simple analogy between the curvature and buoyancy effects.

In Figures 9b and 10b, from the vertical profiles of $\overline{uw}$ at the hill top we can also observe the curvature effects, which are shown by the minimum value of $-\overline{uw}$ near $z = \ell$. Physically, this dip, a rather remarkable aspect of the dynamics, is mainly attributed to the attenuating effect of the convex curvature.

7. Conclusions

We have performed numerical simulations of a turbulent flow over two-dimensional hills with different slopes using a finite-difference method in a non-hydrostatic atmospheric model. Computations of the mean and turbulence flows using the second-order turbulence closure model have been compared with measurements from the EPA wind-tunnel experiment RUSHIL. The results have also been compared with those from an algebraic Reynolds stress model due to Pope. Our findings can be summarized as follows:

1. Previous studies on flow over complex terrain (Taylor et al., 1987; Beljaars et al., 1987; Ayotte et al., 1994) concluded that the simulated results of the mean velocities are insensitive to the turbulence models used. In our study, the simulated mean flow results employing both the second-order closure model and Pope's model all agree well with the measurements, which confirms the general assessment.

2. The simulation results for the turbulence intensities σ_u and σ_w using the second-order closure model are considerably better than those from Pope's model, and generally agree well with the measurements.

3. Pope's formulation fails to predict the shear stress $\overline{uw}$ at hill tops. In order to describe adequately $\overline{uw}$ in hilly terrain, it is necessary to introduce a second-order closure model where the Reynolds stresses are described by transport equations. This finding coincides with the conclusions reached previously (Zeman and Jensen,

1987; Beljaars et al., 1987; Ayotte et al., 1994). The physical reason is that in the outer region, advection of upstream turbulence dominates and only a transport equation for $\overline{uw}$ can realistically model the advection effect. In this study, the second-order closure model gives satisfactory results for $\overline{uw}$ at the hill top.

4. The effects of local equilibrium, rapid distortion and streamline curvature are all shown in the simulation results using the second-order closure model.

From these findings, we conclude that the overall agreement between the second-order closure model predictions and measured data suggests that the fundamental physical mechanisms in the flow over hill case are captured by the model equations.

Acknowledgements

This material is based upon work supported by the U. S. Army Research Office under contract number ARO 195-95. Simulations were produced with the Regional Atmospheric Modelling System (RAMS). RAMS was developed at the Colorado State University under the support of the National Science Foundation (NSF) and the Army Research Office (ARO).

References

Ayotte, K. W., Xu, D. and Taylor, P. A.: 1994, 'The Impact of Different Turbulence Closures on Predictions of the Mixed Spectral Finite Difference Model for Flow over Topography', *Boundary-Layer Meteorol.* **68**, 1–33.

Beljaars, A. C. M., Walmsley, J. L., and Taylor, P. A.: 1987, 'A Mixed Spectral Finite-Difference Model for Neutrally Stratified Boundary-Layer Flow over Roughness Changes and Topography', *Boundary-Layer Meteorol.* **38**, 273–303.

Britter, R. E., Hunt, J. C. R., and Richards, K. J.: 1981, 'Air Flow over a Two-Dimensional Hill: Studies of Velocity Speed-up, Roughness Effects and Turbulence', *Quart. J. Roy. Meteorol. Soc.* **107**, 91–110.

Busch, N. E., Gryning, S. E., Jensen, N. O., and Troen, I.: 1987, 'Turbulence and Diffusion over Inhomogeneous Terrain', *Boundary-Layer Meteorol.* **41**, 173–202.

Clark, T. L.: 1977, 'A Small-Scale Dynamic Model Using a Terrain-Following Coordinate Transformation', *J. Comput. Phys.* **24**, 186–215.

Daly, B. J. and Harlow, F. H.: 1970, 'Transport Equations of Turbulence', *Phys. Fluid* **13**, 2634.

Finnigan, J. J., Raupach, M. R., Bradley, E. F., and Aldis, G. K.: 1990, 'A Wind Tunnel Study of Turbulent Flow over a Two-Dimensional Ridge', *Boundary-Layer Meteorol.* **50**, 277–317.

Gatski, T. B. and Speziale, C. G.: 1993, 'On Explicit Algebraic Stress Models for Complex Turbulent Flows', *J. Fluid Mech.* **254**, 59–78.

Gibson, M. M. and Launder, B. E.: 1978, 'Ground Effect on Pressure Fluctuations in the Atmospheric Boundary Layer', *J. Fluid Mech.* **86**, 491–511.

Hunt, J. C. R., Leibovich, S. and Richards, K. J.: 1988, 'Turbulent Shear Flow over Low Hills', *Quart. J. Roy. Meteorol. Soc.* **114**, 1435–1470.

Irwin, H. P. A. H.: 1974, *Measurements in Blown Boundary Layers*, Ph.D. Thesis, McGill Univ., Montreal.

Jackson, P. S. and Hunt, J. C. R.: 1975, 'Turbulent Wind Flow over a Low Hill', *Quart. J. Roy. Meteorol. Soc.* **101**, 929–955.

Jones, W. P. and Masonge, P.: 1988, 'Closure of the Reynolds Stress and Scale Flux Equations', *Phys. Fluids* **31**, 3589–3604.

Kaimal, J. C. and Finnigan, J. J.: 1994, *Atmospheric Boundary Layer Flows: Their Structure and Measurement*, Oxford University Press, New York, 289 pp.

Khurshudyan, L. H., Snyder, W. H., and Nekrasov, I. V.: 1981, *Flow and Dispersion of Pollutants over Two-Dimensional Hills*, U.S. Envir. Prot. Agcy. Rpt. No. EPA-6000/4-81-067. Res. Tri. Pk., NC., 131 pp.

Khurshudyan, L. H., Snyder, W. H., Nekrasov, I. V., Lawson, R. E. Jr., Thompson, R. S., and Schiermeier, F. A.: 1990, *Flow and Dispersion of Pollutants within Two-Dimensional Valleys: Summary Report on Joint Soviet-American Study*, U.S. EPA Report No. EPA-600/3-90/025, Res. Tri. Pk., NC.

Launder, B. E. and Li, S.-P.: 1994, 'On the Elimination of Wall-Topography Parameters from Second-Moment Closure', *Phys. Fluid* **6**(2), 999–1006.

Launder, B. E., Reece, G. J., and Rodi, W.: 1975, 'Progress in the Development of a Reynolds Stress Turbulence Closure', *J. Fluid Mech.* **68**, 537–566.

Launder, B. E. and Spalding, D. B.: 1974, 'The Numerical Computation of Turbulent Flows', *Comput. Methods Appl. Mech. Eng.* **3**, 269–289.

Mason, P. J. and Sykes, R. I.: 1979, 'Flow over an Isolated Hill of Moderate Slope', *Quart. J. Roy. Meteorol. Soc.* **105**, 383–395.

Newley, T. M. J.: 1985, *Turbulent Air Flow over Hills*, Ph.D. Thesis, University of Cambridge, U.K.

Pope, S. B.: 1975,'A More General Effective-Viscosity Hypothesis', *J. Fluid Mech.* **72**, 331–340.

Prud'homme, M. L.: 1984, *A Reynolds Stress Turbulence Model for Confined Recirculating Flows with Heat Transfer*, Ph.D. Thesis, University of California, Irvine.

Rodi, W.: 1984, *Turbulence Models and Their Application in Hydraulics*, IAHR, Netherlands, 104 pp.

Rotta, J. C.: 1951, 'Statistische Theorie nichthomogener Turbulenz', *Z. Phys.* **129**, 547–572.

Shir, C. C.: 1973, 'A Preliminary Numerical Study of Atmospheric Turbulence Flows in the Idealized Planetary Boundary Layer', *J. Atmos. Sci.* **30**, 1327–1339.

Snyder, W. H., Khurshudyan, L. H., Nekrasov, I. V., Lawson JR, R. E., and Thompson, R. S.: 1991, 'Flow and Dispersion of Pollutants within Two-Dimensional Valleys', *Atmos. Environ.* **25A**, 1347–1375.

Taylor, P. A., Mason, P. I., and Bradley, E. F.: 1987, 'Boundary-Layer Flow over Low Hills', *Boundary-Layer Meteorol.* **39**, 107–132.

Taylor, P. A. and Teunissen, H. W.: 1985, *The Askervein Hill Project: Report on the September/October 1983 Main Field Experiment*, Internal Rep. MSRB-84-6, Atmos. Environ. Service, Downsview, Ontario, Canada.

Taylor, P. A., Walmsley, J. L., and Salmon, J. R.: 1983, 'A Simple Model of Neutrally Stratified Boundary-Layer Flow over Real Terrain Incorporating Wavenumber-Dependent Scaling', *Boundary-Layer Meteorol.* **26**, 169–189.

Walmsley, J. L., Salmon, J. R., and Taylor, P. A.: 1982, 'On the Application of a Model of Boundary-Layer Flow over Low Hills to Real Terrain', *Boundary-Layer Meteorol.* **23**, 17–46.

Walmsley, J. L., Taylor, P. A., and Keith, T.: 1986, 'A Simple Model of Neutrally Stratified Boundary Layer Flow over Complex Terrain with Surface Roughness Modulations (MS3DJH/3R)', *Boundary-Layer Meteorol.* **36**, 157–186.

Xu, D., Ayotte, K. W. and Taylor, P. A.: 1994, 'Development of a Non-Linear Mixed Spectral Finite Difference Model for Turbulent Boundary-Layer Flow over Topography', *Boundary-Layer Meteorol.* **70**, 341–367.

Ying, R., Canuto, V. M., and Ypma, R. M.: 1994, 'Numerical Simulation of Flow Data over Two-Dimensional Hills', *Boundary-Layer Meteorol.* **70**, 401–427.

Ying, R. and Canuto, V. M.: 1995, 'Turbulence Modelling over Two-Dimensional Hills Using an Algebraic Reynolds Stress Expression', *Boundary-Layer Meteorol.* **77**, 69–99.

Zeman, O. and Jensen, N. O.: 1987, 'Modification of Turbulence Characteristic in Flow over Hills', *Quart. J. Roy. Meteorol. Soc.* **113**, 55–80.